한국환경과학회지 제5권(제5호), 593~603, 1996
J. of the Korean Environmental Sciences Society

Modified Agglomerated Film Model Applied to a Molten Carbonate Fuel Cell Cathode

Jun-Heok LIM, Tae-Keun KIM*
Dept. of Chemical Engineering, Pukyong National University, Pusan, 608-737, Korea
**Dept. of Environmental Engineering, Pukyong National University, Pusan, 608~737, Korea*
(Manuscript received 10 August 1996)

A dual-porosity filmed agglomerate model for the porous cathode of the molten carbonate fuel has been investigated to predict the cell performance. A phenomenological treatment of molecular, kinetic and electrode parameters has been given. The major physical and chemical phenomena being modeled include mass transfer, ohmic losses and reaction kinetics at the electrode-electrolyte interface. The model predicts steady-state cell performance, given the above conditions that characterize the state of the electrode. Quasi-linearization and finite difference techniques are used to solve the coupled nonlinear differential equations. Also, the effective surface area of electrode pore was obtained by mercury porosimeter. The results of the investigation are presented in the form of plots of overpotential vs. current density with varied the electrode material, gas composition and mechanism. The predicted polarization curves are compared with the empirical data from 1 cm^2 cell. A fair correspondence is observed.
Key words : Molten Carbonate Fuel Cell, Electrode, Model, Cathode

1. INTRODUCTION

The construction and development of fuel cells comprises considerable technology and is already a subject of monographs. Basically a fuel cell is an electrochemical cell and an open system which can continuously transform the chemical energy of fuel and oxidant to electrical energy by a process involving an essentially invariant electrode-electrolyte system. Fuel cell reactants are converted into chemical products and electricity without the prospect of being regenerated. (Appleby and Foulkes (1989), Bockris and Srinivasan (1969))

Fuel cell efficiency is not Carnot-limited; an energy efficiency of 65~70% is feasible for electricity generation, compared to 30~35% for a conventional Carnot limited coal burning power plant. A rough division of present-day fuel cells may be made according to the temperature of operation. Thus if this is above about 500℃, the device is called a high-temperature fuel cell. For the high-temperature cells, the temperature alone causes the electrode kinetics to be sufficient rapid that there can be production of energy at suitable rate without using expensive materials as catalysts. Molten carbonate fuel cells are operated at 650℃ and have a semi-solid carbonate paste as electrolyte. The basic electrochemical reactions in a molten carbonate fuel cell are as follows:

Anode (fuel electrode)

$$H_2 + CO_3^{-2} \leftrightarrows CO_2 + 2e^- \quad (1-1)$$

Cathode (oxygen electrode)

$$CO_2 + 1/2\ O_2 + 2e^- \leftrightarrows CO_3^{-2} \quad (1-2)$$

Overall reaction

$$H_2 + 1/2\ O_2 \leftrightarrows H_2O \quad (1-3)$$

At the anode, which is a porous gas diffusion electrode, hydrogen molecules in molten carbonates electrolyte adsorbed on the electrode surface and react with carbonate ions to form water and car-

bon dioxide. These products then go through the reverse mass transfer processes back to the gas phases.

The cathode consists of porous nickel oxide (gas diffusion electrode), which has a low electrical conductivity. The conductivity of cathode is improved by lithium doping ("lithiation") upon contact with the melt. Porous electrodes promote intimate contact of the electrode material with the electrolyte and gaseous phase. A large interfacial area per unit volume is provided when gas-diffusion electrodes are used.

It is necessary to establish a model which accounts for the essential features of an actual electrode without going into exact geometric detail. The first objective of the model is to predict the performance of the fuel cell. The performance of fuel cell is the current density and the available cell potential, as a function of gas flow rates and compositions, external load, electrode thickness, pore size and temperature.

Several models have been developed in the past twenty years to explain the behavior of porous gas diffusion electrode. Austin et al (1965) proposed simple pore model. This model is too simple and predicts too low mass transport-limited current. Will et al (1969) introduced the thin film model and Hurwitz and Srinivasan (1967) applied this model to fuel cells with the consideration of activation control. Brown (1966) proposed a composite of thin film and flooded pore model (agglomerated model). It is assumed that the metallic portion consists of porous agglomerates and that the porous metallic particles are coated by a thin film. Gunter and Hunter (1969) developed a simple agglomerated model. Models for molten carbonate fuel cell electrode have been published by Yuh et al (1984), Lee et al (1993), Kunz et al (1984), and Bergman et al 1(1992). In this work, the film agglomerate porous-electrode model has been employed and modified for the cathodes, using surface kinetic expressions such as the ones discussed above. The objective of the research is to predict the performance of molten carbonate fuel cell cathodes and obtain the optimum cathode condition.

2. THEORY

2-1. Electrode kinetics of oxygen reduction

Adequate study of oxygen reduction kinetics are available only on gold electrodes. The dependency of the exchange current density, i_0^b, on reactants and products concentration were investigated by Appleby and Foulkes (1989). They proposed following two mechanisms. (*means rate determining step)

i) Peroxide mechanism

$$\frac{1}{2}O_2+CO_3^{2-} \leftrightarrows CO_2+O_2^{2-}$$
$$O_2^{2-}+e^- \longrightarrow O^{2-}+(O^-)\ * \qquad (2\text{-}1)$$
$$(O^-)+CO_2+e^- \rightleftarrows CO_3^{2-}$$
$$O^{2-}+CO_2 \rightleftarrows CO_3^{2-}$$

This mechanism predicts $\alpha_a=1.5$, $\alpha_c=0.5$ and

$$i_0^b \propto (O_2)^{0.375}\ (CO_2)^{-1.25} \qquad (2\text{-}2)$$

ii) Superoxide mechanism

$$3O_2+2CO_3^{2-} \rightleftarrows 2CO_2+4O_2^-$$
$$O_2^{2-}+e^- \longrightarrow O^{2-}+(O^-) \qquad (2\text{-}3)$$
$$O_2^-+e^- \rightleftarrows O_2^{2-}\ *$$
$$O^{2-}+CO_2 \rightleftarrows CO_3^{2-}$$

This mechanism predicts $\alpha_a=0.5$, $\alpha_c=0.5$ and

$$i_o^b \propto (O_2)^{0.625}\ (CO_2)^{-0.75} \qquad (2\text{-}4)$$

2-2. Filmed agglomerate model

As shown in Fig. 1-(a), the electrode structure can be pictured as one in which catalyst particles from agglomerates which, under working conditions, are flooded with electrolyte. The existence of a surface film on the external surface of the agglo-

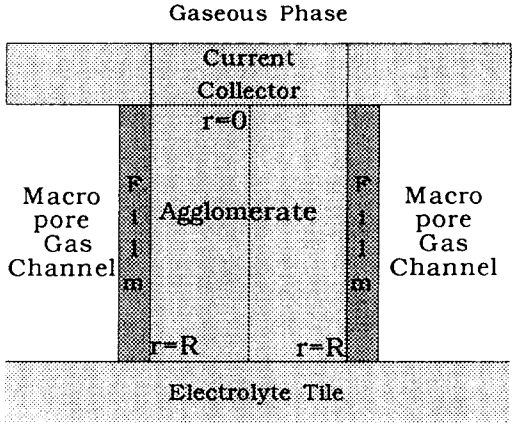

(a)

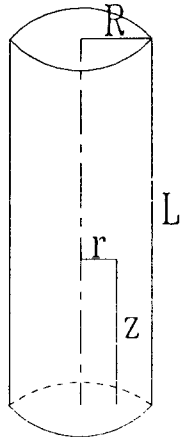

(b)

Fig. 1. (a) Schematic structure of porous electrode in film agglomerate models. (b) detailed structure of agglomerate.

merate depends on the wetting characteristics of the electrolyte. It is very likely that such a film exists in the cathode (NiO). It is likely that an electrolyte film exists on the cathode agglomerate. Therefore, we have to develop a "Filmed Agglomerate Model" to apply specifically to cathode. One make the following assumptions in order to simplify the mathematical analysis without going into the actual geometry within the agglomerates.

1. The electrode is made up of a number of cylinders of catalyst with radius R and length L as shown in Fig. 2-(b). The agglomerate are flooded with electrolyte. These cylinders are perpendicular to the external surface of the electrolyte tile.
2. The electrolyte and catalyst are homogeneous mixed as a continuum and all the kinetic parameters are constant.
3. There is no electronic IR-drop in the metal phase due to much higher electric conductivity of cathode material compared to the molten carbonate melt.
4. The voltage in the cylinder changes only in the axial direction and diffusion of dissolved gas occurs only in the radial direction. Also, the transport of current through the electrolyte follows ohm's law.
5. The composition of the gas phase is uniform.
6. The electrode operates isothermally and isobarically with constant transport properties.
7. The activity of CO_3 ion is everywhere equal to unity.

The following generalized reaction takes place at the electrode surface.

$$\Sigma S_i M_m^{zi} \rightarrow ne^- \qquad (2\text{-}5)$$

Where S_i denotes the stoichiometric coefficient. One starts by making a current balance over a differential section of the cylinder. The material balance for species i can be expressed as

$$\nabla \cdot N_i = -\frac{S_i A i_n}{n.F} \qquad (2\text{-}6)$$

where in is the transfer current density at the electrode-electrolyte interface due to the electrochemical reaction and N_i is the mass flux of species i. A is the specific surface area of the agglomerate (cm^2cm^3). The flux is related to concentration gradient:

$$N_i = -\overline{D_i} \cdot \nabla C_i \qquad (2\text{-}7)$$

where C_i is the concentration of species i in the electrolyte phase and Di is the effective diffusion coefficient. Substituting equation (2-7) into equation (2-6) yields

$$= \overline{D_i} \nabla^2 C_i \frac{S_i A_{in} i_n}{nF}, \ \overline{D_i} \frac{\varepsilon_m}{\tau} D_i \qquad (2\text{-}8)$$

In dimensionless cylindrical coordinates,

$$\left[\frac{1}{\xi} \frac{\partial}{\partial \xi} \left(\xi \frac{\partial \overline{C_i}}{\partial \xi} \right) + \frac{R^2}{L^2} \frac{\partial^2 \overline{C_i}}{\partial \xi^2} \right] = \frac{R^2 S_i A i_n}{nFD_i C_i^b} \qquad (2\text{-}9)$$

$$\text{where } \overline{C_i} = \left(\frac{C_i}{C_i^b} \right), \xi = \left(\frac{\gamma}{R} \right), \xi = \left(\frac{Z}{L} \right) \qquad (2\text{-}10)$$

Since $R^2/L^2 << 1$ and $\frac{\partial^2 \overline{C_i}}{\partial \xi^2}$ and $\frac{1}{\xi} \frac{\partial}{\partial \xi} \left(\xi \frac{\partial \overline{C_i}}{\partial \xi} \right)$ are approximately of the same order, we can neglect the $\frac{R^2}{L^2} \frac{\partial^2 \overline{C_i}}{\partial \xi^2}$ term. As a result we have

$$\frac{1}{\xi} \frac{\partial}{\partial \xi} \left(\xi \frac{\partial \overline{C_i}}{\partial \xi} \right) = \frac{R^2 S_i A i_n}{nF \overline{D_i} C_i^b} \qquad (2\text{-}11)$$

In case of $S_1 = -1$ (O_2) :

$$\frac{1}{\xi} \frac{\partial}{\partial \xi} \left(\xi \frac{\partial \overline{C_i}}{\partial \xi} \right) = \frac{R^2 S_1 A i_n}{nF \overline{D_1} C_1^b} \qquad (2\text{-}12)$$

In case of $S_2 = -2$ (CO_2) :

$$\frac{\partial}{\partial \xi} \left(\xi \frac{\partial \overline{C_1}}{\partial \xi} \right) = \frac{S_1 \overline{D_2} C_2^b}{nF \overline{D_1} C_1^b} \frac{\partial}{\partial \xi} \left(\xi \frac{\partial \overline{C_2}}{\partial \xi} \right) \qquad (2\text{-}13)$$

In the following the subscript 1 stands for O_2 and 2 for CO_2. The total current output per superficial cm^2 is I times the total number of agglomerates per cm^2. Since the reference electrode is situated in the electrolyte tile, the polarization at $\xi = 1$ can be know from there. The current density vs. polarization diagram is the final result of this model.

With a film on the external surface of the agglomerate, the diffusion equation (2-12) and (2-13) are unchanged within the agglomerates. Due to the diffusion limitation caused by the existence of a film, there is no chemical reaction in film, the diffusion equations are simply:

$$\frac{1}{\gamma} \frac{\partial}{\partial \gamma} \left(\gamma \frac{\partial C_i}{\partial \gamma} \right) = 0 \text{ (cylindrical coordinate)} \qquad (2\text{-}14)$$

which neglects the axial diffusion term. Then, we can integrate (2-14) as

$$\gamma \frac{\partial C_i}{\partial \gamma} = \frac{C_i^b - C_i^s}{\Delta}, \ \Delta = \ln \left(\frac{R+\delta}{R} \right) \qquad (2\text{-}15)$$

$$\text{at } \gamma = R, \left(\frac{\partial C_i}{\partial \gamma} \right) = \frac{C_i^b (1 - \overline{C_i^s})}{R\Delta}$$

The diffusion flux within the film toward the agglomerate can be computed from equation (2-15). Next, we have to make the material balance at $\xi = 1$ to have the appropriate boundary condition there. For species i, the diffusion flux in the film toward the surface equals the depletion rate on the external surface plus the diffusion flux toward the interior of the agglomerate. In mathematical dimensionless form is,

$$\left(\frac{\partial C_i}{\partial \xi} \right) - F' (1 - \overline{C_i}) + P_i'' i_n = 0 \text{ (at } \xi = 1) \qquad (2\text{-}16)$$

$$\text{where } F' = \frac{1}{\varepsilon \Delta}, \ P_i'' = \frac{2 S_i (1-\varepsilon) R}{n F C_i^b \overline{D_i}} \qquad (2\text{-}17)$$

The potential equation has to be described in equation (2-18) because the film can conduct current as well as the agglomerate.

$$\frac{dj}{dz} = \frac{n F C_i^b \overline{D_i}}{(R+\delta)^2 \Delta} (1 - \overline{C_i^s}) \qquad (2\text{-}18)$$

The current density is

$$j = \frac{I}{\pi (R+\delta)^2} = -x \frac{\left(R^2 + \frac{[(R+\delta)^2 - R^2]}{\varepsilon} \right)}{(R+\delta)^2} \frac{d\phi_L}{dZ} \qquad (2\text{-}19)$$

Substituting equation (2-19) into equation (2-18)

and nondimensionalize it, one has

$$\frac{d^2\psi_L}{d\xi^2}=-\frac{n\,F\,D_1\,C^b_1\,\phi^2_L}{\chi\,R_1\,(R+\delta)^2\triangle}(1-\overline{C_i^s}) \tag{2-20}$$

The current output per agglomerate can now be computed from the potential gradient.

$$I=(Q+Q')\frac{d^2\psi_L}{d\xi^2} \tag{2-21}$$

$$Q'=-\frac{\chi\pi[(R+\delta)^2-\gamma^2]}{\phi_L}$$

The general Butler-Volmer equation is:

$$i_n=i^o_o(\overline{C_1})^{\alpha}(\overline{C_2})^{\beta}\left[e\left(\frac{a_aF}{RT}\right)\eta_s-e\left(\frac{-a_aF}{RT}\right)\eta_s\right] \tag{2-22}$$

With the boundary conditions at $\xi=1$ and differential equations (2-12) and (2-13), the equation (2-22) becomes

$$\left(\frac{\partial\overline{C_i}}{\partial\xi}\right)-F'(1-\overline{C_i})+P''_i\,i_n=0\ (\text{at }\xi=1) \tag{2-23}$$

$$\text{where}\quad F'=\frac{1}{\varepsilon\triangle},\ P''_i\,i_n=\frac{S_i(1-\varepsilon)\,R}{4\,F\,C^b_i\,\overline{D_i}} \tag{2-24}$$

Next we have to develop the relationship between Φ_L, $\eta_{s,c}$ and $\eta_{s,k}$. At the cathode, we can use Nernst equation. If the activities of all species are all zero, the standard equilibrium potential can be obtained by

$$\eta_{s,k}=-\Phi_L-V^o_{oc}-\frac{1}{2\phi}\ln\left(\overline{C_1}^{\frac{1}{2}}\overline{C_2}\right) \tag{2-25}$$
$$\Psi=(V^o_{oc}-\Phi_L)\,\phi$$

Substituting equation into equation (2-12) and (2-13), one has

$$\frac{1}{\xi}\frac{\partial}{\partial\xi}\left(\xi\frac{\partial\overline{C_i}}{\partial\xi}\right)+\left(G1(\overline{C_1})^{\alpha-\frac{\alpha_a}{2}}(\overline{C_2})^{\beta-\frac{\alpha_a}{2}}\exp(-\alpha_a\psi_c)\right. \tag{2-26}$$
$$\left.-G1(\overline{C_1})^{\alpha-\frac{\alpha_c}{2}}(\overline{C_2})^{\beta-\frac{\alpha_c}{2}}\exp(\alpha_c\psi_c)\right)=0\quad(i=1)$$

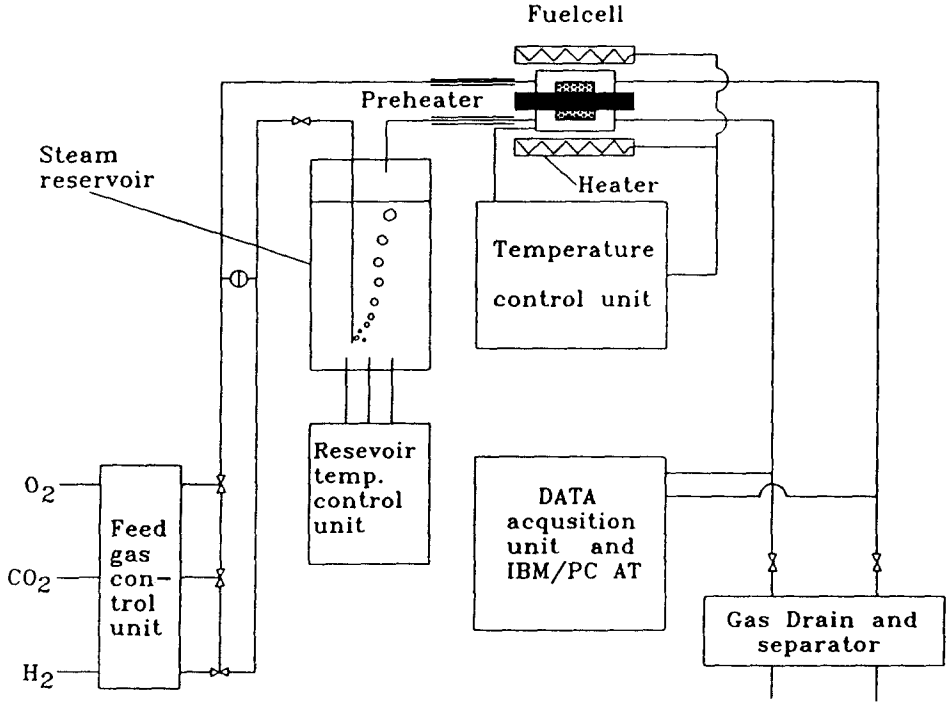

Fig. 2. Schematic diagram of laboratory MCFC unit/half cell.

$$\frac{1}{\xi}\frac{\partial}{\partial\xi}\left(\xi\frac{\partial\overline{C_1}}{\partial\xi}\right)-\frac{s_1}{s_2}k_2\frac{\partial}{\partial\xi}\left(\xi\frac{\partial\overline{C_2}}{\partial\xi}\right)=0\ (i=2) \tag{2-27}$$

where $G1=\dfrac{A\,R^2\,i^0_0}{C^{b1}\,\overline{D_1}\,(4F)}$ (2-28)

The potential and current density related in

$$\frac{\partial^2\Psi_c}{\partial\delta^2}=\frac{-2nFD_1C^b{}_1\phi L^2}{\overline{\chi}R_1(R+\delta)^2\triangle S_1}(1-\overline{C_1}^s) \tag{2-29}$$

We have three nonlinear coupled partial differential equations which need to be solved by some appropriate numerical method. The potential is only a function of z. We can solve the diffusional equations (2-26) and (2-27) for the cathode with a specified value of Ψ which depends on z through equation (2-29).

3. EXPERIMENT

A laboratory-scale fuel cell assembly is shown in Fig. 2. Gold reference electrode which consists of a gold wire (0.5 mm, 99.9%) in an 1/8" alumina tube containing electrolyte, and sparged by gas. A 33% $O_2$67% CO_2 gas mixture is used as the reference gas. Liquid contact with the main electrolyte is established by means of a 0.5 mm hole in bottom of alumina tube. The electrolyte, which is usually a eutectic of Li_2CO_3 and K_2CO_3, or a ternary (Li-Na-K) CO_3 eutectic, is held by capillary force within the voids of a lithium aluminate "tile".

This tile prevents recombination of a lithium aluminate. Also, this tile prevents recombination of the reactant gases and slows down the electrolyte vaporization loss. The structure of the tile must be carefully chosen to avoid the flooding of electrode macropores, which would create a vary large unfavored mass transfer resistance. The lithium aluminate tile is fabricated by tape casting of carbonate power and finely divided γ-Al_2O_3 with Al_2O_3 fiber.

Table 1 show the characteristics of the components, used in this experiment. The cathode of MCFC is fabricated by tape casting of metal powder (NiO) and cold pressing of oxide powder (perovskite, $La_{0.8}Sr_{0.2}CoO_3$).

4. RESULTS AND DISCUSSION

The filmed agglomerate model was useful to predict the performance of NiO and perovskite ($La_{0.8}Sr_{0.2}CoO_3$) cathode in MCFC. The theoretical effect of operating conditions (gas composition, catho-

Table 1. The specification of MCFC unit cell component

	Cathode	Anode	Electrolyte	Electrolyte matrix
Material	$La_{0.8}Sr_{0.2}CoO_3$ NiO	Ni	$Li_2CO_3K_2CO_3$ (62:38)	$LiAlO_2+Al_2O_3$ fiber
Thickness (mm)	0.8~1.0	0.7	0.2	1.0~1.5
Porosity (%)	50~65	65~70	-	-
Surface area (m^2/g)	-> 1.32~2.20 -> 0.56	8.89	-	-
Fabrication	Cold pressing or paste loading	Paste loading	Tape casting	Tape casting
Operating condition	in-situ oxidation	Sintering	in-situ sintering	in-situ sintering

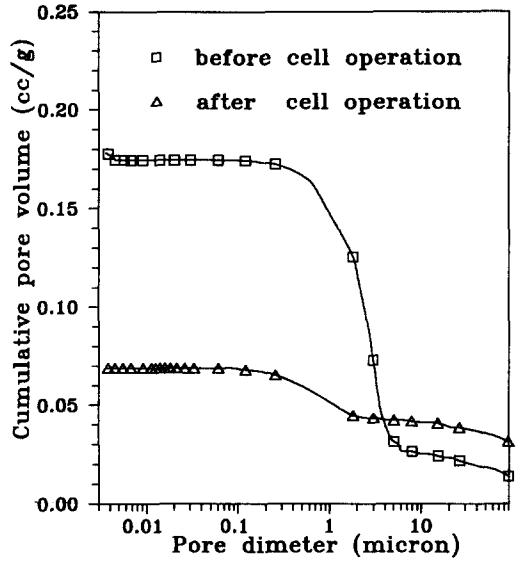

Fig. 3. Pore size distribution of MCFC cathode (Before and after cell operation)

dic reaction mechanism, film thickness, electrode thickness and electrode material) were discussed. Also, the comparison of experimental and theoretical cell performance was performed in this study.

4-1. Parametric study

At the beginning of filmed agglomerate model study, Selman et al (1984, 1993) calculate the agglomerate radius and effective surface area by ordered cylinder geometry. It used generally by other researchers. Though, the ordered cylinder geometry is easy to calculate, it is hard to decide the agglomerate size. Fig. 3 show the pore size distribution of molten carbonate fuel cell cathode before and after the fuel cell experiment. The drastic decrease of micro pore volume was observed in Fig. 3. The difference of volume change before and after the cell operation is mainly due to the electrolyte filling in micro pore. The wettability of electrolyte in oxide cathode is very high. During the cell operation, electrolyte might be cover the agglomerate surface and fills micro pore. So, we can estimate the effective surface area of filmed agglomerate model at the hump of cumulative pore volume after the cell operation.

If the pore shows a capillary behavior, we can apply the Young & Laplace equation. In cylindrical agglomerate, the relation of agglomerate radius, electrolyte volume in pore and surface area can

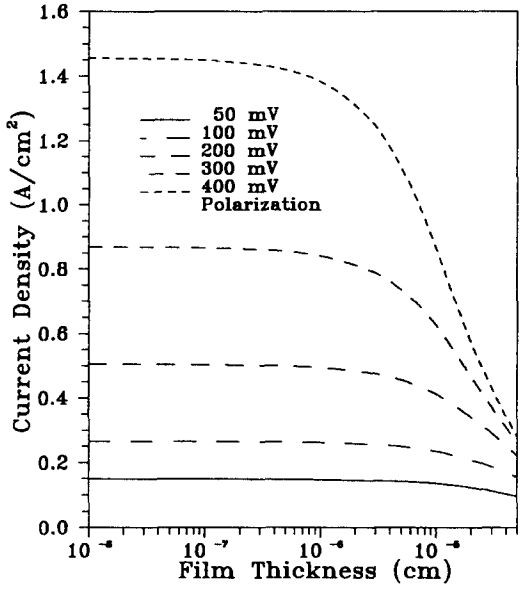

Fig. 4. The effect of electrolyte film thickness on the predicted polarization curve of MCFC cathode by peroxide mechanism

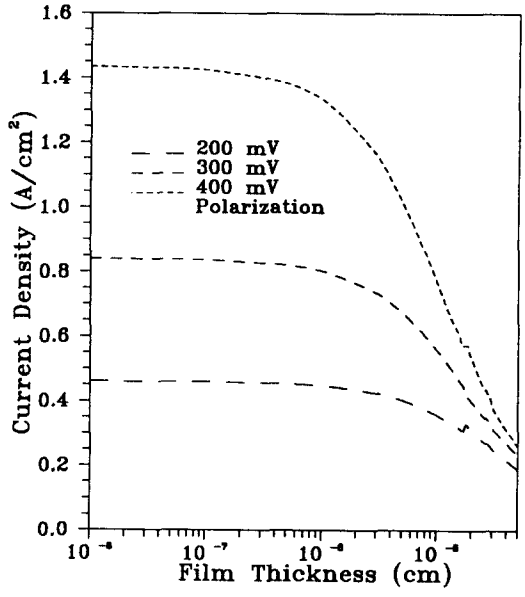

Fig. 5. The effect of electrolyte film thickness on the predicted polarization curve of MCFC cathode by superoxide mechanism

be presented by next equation.

$$\frac{A}{V_{filled}} = \frac{2}{\gamma_0} \tag{4-1}$$

$$\gamma_0 = \frac{V_{filled}}{\int_{V_{filled}}^{V_{total}} \frac{dV}{\gamma}} \tag{4-2}$$

$$\theta_A = \frac{V_{filled}}{V_{filled} + V_{solid}} \tag{4-3}$$

$$N = \frac{V_{filled} + V_{solid}}{\pi \gamma_0^2 L} \tag{4-4}$$

The effect of overpotential and film thickness on the concentration profiles were shown in Fig. 4 and Fig. 5. Larger overpotentials and thicker films both result in smaller surface oxygen concentration. A larger overpotential also yields smaller oxygen concentrations in the core region where film thickness variations have a much smaller effect. The higher the value of film thickness, the higher the diffusion limitation in the film. Thicker films may make the lower exchange current densities.

Because the film is highly conductive, we can expect that the overpotential distribution is more uniform than that in the case without film. Thin films increase ohmic resistance and reaction rate, thereby yielding a more nonuniform overpotential distribution. In Fig. 4 and Fig. 5, the high polarization tends to make the overpotential more nonuniform but this effect may be negligibly small in practical cell operation. It is suggested that, a thinner film and a higher exchange current density yield better electrode performance, in agreement with qualitative predictions.

The effect of electrode thickness on the exchange current density were shown in Fig. 6. The cell performance was increase with the cathode thickness in the range of 0 to 4 mm. More thick electrode result in lower cell performance. The effect of agglomerate porosity on the exchange current density were shown in Fig. 7. Bergman et al (1992) reported that the active surface area varies inversely to the agglomerate radius but only weaker than inversely to the square root of the particle radius. In order to increase the activity of the electrode it is therefore more effective to decrease the agglomerate radius than the particle size. This is

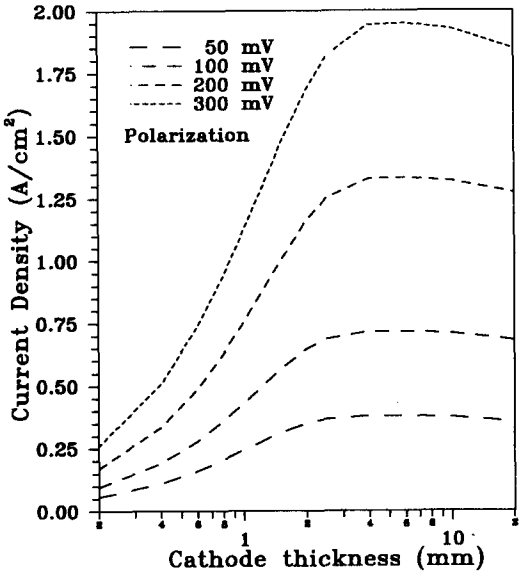

Fig. 6. The effect of cathode thickness on the predicted polarization curve of MCFC cathode

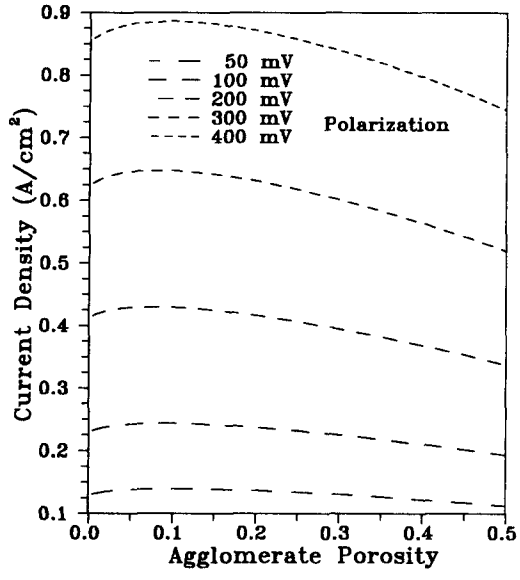

Fig. 7. The effect of agglomerate porosity on the predicted polarization curve of MCFC cathode

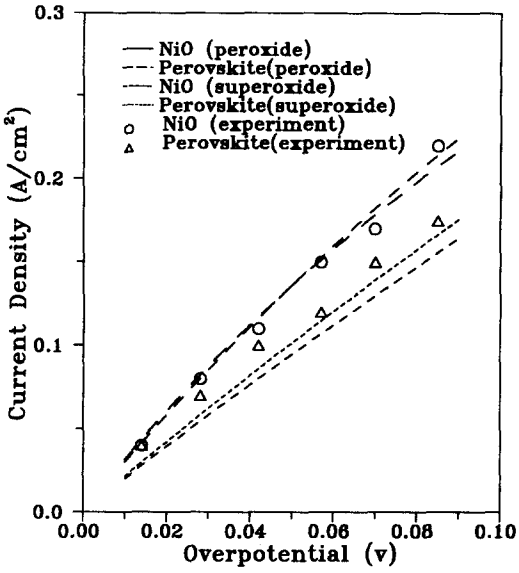

Fig. 8. Measured and calculated polarization curve of perovskite ($La_{0.8}Sr_{0.2}CoO_3$) and NiO cathode (O_2/CO_2=0.15/0.3, peroxide and superoxide mechanism)

a direct implication of the fact that under pore diffusion limiting conditions, the electrochemical reaction is squeezed to a thin zone close to the agglomerate surface. As a matter of fact, Fig. 7 shows that only the utmost particle layer of the agglomerate is utilized for the electrochemical reaction.

4-2. Fitting on experimental data

Fitting experimental data to the filmed agglomerate model may be considered a practical engineering approach to finding the kinetic parameters of oxygen reduction at a perovskite ($La_{0.8}Sr_{0.2}CoO_3$) and nickel oxide cathode. Cathodic data from half cell using a perovskite ($La_{0.8}Sr_{0.2}CoO_3$) and nickel oxide cathode are fitted assuming either a peroxide or a superoxide mechanism. No film thicknesses have been experimentally determined up to now. The only way to estimate is to fit the polarization curve with the lowest oxygen mole fraction whose limiting current can be determined easily. The film thickness thus determined does not depend on electrode kinetics because the only limitation is the diffusion limitation in the film. In this work it is assumed that the film thickness determined in this way is independent of gas compositions. This may not be true in practice, but it is a highly convenient assumption in the case of molten carbonate fuel cell electrodes, which are practically inaccessible. So, the film thickness was calculated by the theory of Mitteldorf and Wilemski (1969).

The experimental data of half cell was compared with theoretical result in Fig. 8. As a result, the peroxide mechanism appears to give a better fit than the superoxide mechanism in NiO cathode. In case of NiO, the superoxide mechanism predicts low exchange current density. In case of perovskite ($La_{0.8}Sr_{0.2}CoO_3$), the experimental data was tend to intermediate of both mechanism. Detailed investigation was needed in perovskite ($La_{0.8}Sr_{0.2}CoO_3$) cathode.

5. CONCLUSIONS

1. The modified filmed agglomerate model combined with the real pore size distribution data, gives a good fit to cathodic data with peroxide mechanism. Superoxide mechanism predicts low current density at a given polarization.
2. The half cell test showed similar performance in perovskite and NiO. It was found that the thickness, electrode porosity and agglomerate porosity of perovskite cathode was optimum at 1.5~2 mm, 65% and 12% respectively.

Nomenclature

a : superficial surface area cm^2
A_{in} : internal cathode surface area cm^2/cm^3
C_i^b : equilibrium concentration at electrolyte and gas interface mol/cm^3
Cis : equilibrium concentration at electrode surface mol/cm^3
F : faraday constant C/g-eq
iL : local current density in electrolyte phase A/cm^2
iob : exchange current density A/cm^2
L : agglomerate length cm
N : agglomerate number dimensionless

R, r_o : agglomerate radius cm
R_O : radius of oxygen ion μm
V_{filled} : electrolyte volume in cathode pore cm^3
V_{total} : superficial volume of cathode cm^3
V_{solid} : true material volume of cathode cm^3

Greek symbol

α_A : anodic transfer coefficient
α_C : cathodic transfer coefficient
δ : electrolyte film thickness at agglomerate surface μm
Δ : ln ((R % δ)/R) dimensionless
ε, θ_A : agglomerate porosity dimensionless
η : *overpotential* V
η_s : local surface overpotential V
θ : electrode porosity dimensionless
Φ_o : potential at electrolyte matrix and electrode interface V
Φ_L : potential at electrolyte phase V

REFERENCES

A. J. and F. R. Foulkes, 1989; Fuel Cell Handbook, Van Nostrand Reinhold, NEW YORK.

Austin L.G., M. Ariet, R.D. Walker, G.B. Wood and R.H. Comyn, 1965; Simple Pore and Thim Film Models of Porous Gas-Diffusion Electrodes, I & EC Fundamentals, *4 (3)*, 321~327.

Bergman B., E. Fontes, C. Lagergren and D. Simonsson, 1992; Mathematical Modelling of the MCFC Cathode, Fuel Cell Seminar Abstract, Tucson, USA.

Bockris J.O.M. and S. Srinivasan, 1969; Fuel Cells : Their Electrochemistry, McGraw-Hill Inc., New YorkBrown R. and J.A. Rockett, 1966; Theory of the Performance of Porous Fuel Cell Electrodes, J. of Electrochemical Society, *113 (3)*, 207~213.

Mitteldorf J. and G.Wilemski, 1969; Film Thickness and Distribution of Electrolyte in Porous Fuel Cell Components, J. of Electrochemical Society, *131 (8)*, 1784.

Ginter J. and C. Hunter, 1969; The Mechanism of Operation of the Teflon-Bonded Gas Diffusion Electrode, J. of Electrochemical Society, *116 (8)*, 1124.

Yuh C.Y. and J. R. Selman, 1984; Polarization of the Molten Carbonate Fuel Cell Anode and Cathode, J. of Electrochemical Society, *31 (9)*, 2062.

Lee G.L., L. Pomp and J. R. Selman, 1993; Comparison of MCFC Cathode Materials by Porous Electrode Performance Modeling, J. of Electrochemical Society, *140 (2)*, 390.

Kunz H.R., L. J. Bregoli and S. T. Szymanski, 19 84; A Homogeneous/Agglomerate Model for Molten Carbonate Fuel Cell Cathodes, J. of Electrochemical Society, *131 (12)*, 2815.

Srinivasan S. and H.D. Hurwitz, 1967; Theory of a Thin Film Model of Porous Gas-Diffusion Electrodes, Electrochimica ACTA, *12*, 495.

Will F.G. and D.J. Ben Daniel, 1969, Significance of Electrolyte Films for Performance of Porous Hydrogen Electrodes, J. of Electrochemical Society, *116 (7)*, 933~937.

실측자료를 이용한 Agglomerated Film Model의 용융탄산염 연료전지 산소전극 성능모사

임준혁 · 김태근*
국립부경대학교 공과대학 화학공학과
국립부경대학교 공과대학 환경공학과
(1996년 8월 10일 접수)

용융탄산염 연료전지의 산소전극성능모사를 위한 이중기공구조의 filmed agglomerate model을 연구하였다. 이 모델에서는 전극과 전해질 계면의 물리, 화학적인 현상 및 전극반응기구를 고려하여 정상상태에서 전극의 특성을 조업조건에 따라 표시할 수있다. 기존의 연구에서 기하학적인 구조를 가정하여 전극반응면적을 이론적으로 계산한 반면에 본 연구에서는 porosimeter를 이용한 기공도와 기공구조 분포 측정자료를 이용한 방법을 제시하였다. 계산결과는 전극재질, 기체조성, 전극두께, agglomerate 기공도 및 전해질 막의 두께에 따른 영향을 전류밀도와 과전압의 관계로 표시하였다. 또한 전극 재질로 perovskite ($La_{0.8}Sr_{0.2}CoO_3$)와 NiO를 사용하여 실제전지를 이용한 성능을 측정하여 이론치와 비교하였다. 두전극의 반쪽전지 실험에서 유사한 성능을 나타내었다. Perovskite 전극은 전극 기공도 65%, agglomerate 기공도 12% 그리고 전극두께 1.5~2 mm에서 최적의 결과를 보여주었다. NiO전극의 경우 peroxide 반응기구에서 superoxide 반응기구의 계산결과보다 실험치와 일치하는 좋은 결과를 보였다.